J. Fluid Mech. (1989), *vol.* 203, *pp.* 77–101
Printed in Great Britain

An algebraic model for the turbulent flux of a passive scalar

By MICHAEL M. ROGERS†, NAGI N. MANSOUR† AND WILLIAM C. REYNOLDS‡

† NASA Ames Research Center, Moffett Field, CA 94035, USA

‡ NASA Ames Research Center, Moffett Field, CA 94035, USA *and* Department of Mechanical Engineering, Stanford University, Stanford, CA 94305, USA

(Received 4 November 1987 and in revised form 8 September 1988)

The behaviour of passive-scalar fields resulting from mean scalar gradients in each of three orthogonal directions in homogeneous turbulent shear flow has been studied using direct numerical simulations of the unsteady incompressible Navier–Stokes equations with $128 \times 128 \times 128$ grid points. It is found that, for all orientations of the mean scalar gradient, the sum of the pressure–scalar gradient and velocity gradient–scalar gradient terms in the turbulent scalar flux balance equation are approximately aligned with the scalar flux vector itself. In addition, the time derivative of the scalar flux is also approximately aligned with the flux vector for the developed fields (corresponding to roughly constant correlation coefficients). These alignments lead directly to a gradient transport model with a tensor turbulent diffusivity. The simulation results are used to fit a dimensionless model coefficient as a function of the turbulence Reynolds and Péclet numbers. The model is tested against two different passive-scalar fields in fully developed turbulent channel flow (also generated by direct numerical simulation) and is found to predict the scalar flux quite well throughout the entire channel.

1. Introduction

Turbulent mixing is of great importance in engineering applications. In reacting flows, turbulent mixing often controls the rate of reaction. Predicting the behaviour of contaminants requires a knowledge of turbulent mixing characteristics. The dispersion of contaminants or internal energy (with small temperature variations) are examples of transport of a passive scalar that is convected by and diffuses through the hydrodynamic field without modifying it in any way.

Solution of the Reynolds-averaged mean passive-scalar equation requires modelling the turbulent passive-scalar flux. Gradient transport models have been used to model turbulent fluxes of momentum and passive scalars since Boussinesq (1877). By analogy with molecular transport, these models relate the turbulent flux linearly to the mean gradient of the transported property. The constant of proportionality is then termed an 'eddy' or 'turbulent' diffusivity. Such a simple algebraic representation of the turbulent transport permits closure of the Reynolds-averaged mean scalar-field equation.

Richardson (1920) noted that the turbulent diffusivity in turbulent shear flow has a different value for different orientations of the mean scalar gradient. To describe this behaviour it is necessary to describe the turbulent diffusivity by a second rank tensor. In general there is no reason to expect the scalar flux and the mean scalar

gradient to be aligned (indeed experimental and numerical work on shear flow show this not to be the case) and, because of this, the diffusivity tensor does not have to be diagonal.

Corrsin (1974) has voiced reservations about the self-consistency of gradient transport models with spatially varying turbulent diffusivities. It is clear, however, that for gradient transport models to work in inhomogeneous flows one must permit a spatial dependence of the turbulent diffusivity. This can be easily seen in fully developed channel flow with scalar transfer in one wall and out the other. In this flow a constant turbulent diffusivity would be consistent only with a linear mean scalar profile. Although this is a good approximation throughout the centre of the channel it is not the case in the near-wall region.

The objective of this work is to develop an algebraic gradient transport model for the turbulent flux of a passive scalar in turbulent shear flows from a database generated by direct numerical simulation of the Navier–Stokes equations. To model the full diffusivity tensor, passive-scalar fields resulting from mean scalar gradients aligned with each of the coordinate directions are considered separately. In order to permit predictions in inhomogeneous flows, the turbulent diffusivity tensor can exhibit a spatial dependence.

In §2, the governing equations and the numerical simulations used in this work are discussed. In addition, a brief description of the behaviour of passive-scalar fields in homogeneous turbulent shear flow is given. Section 3 describes the development of a model for the turbulent passive-scalar flux using the results of the homogeneous turbulent shear flow simulations, and §4 discusses the model's performance in an inhomogeneous turbulent flow (fully developed turbulent channel). A summary of results and conclusions is given in §5.

2. The simulations

2.1. *The governing equations*

The equations governing the flow and a passive scalar in an incompressible Newtonian fluid are

$$U_{i,i} = 0, \tag{2.1}$$

$$\frac{\partial U_i}{\partial t} + U_j U_{i,j} + \frac{1}{\rho} P_{,i} = \nu U_{i,jj}, \tag{2.2}$$

$$\frac{\partial T}{\partial t} + U_j T_{,j} = \gamma T_{,jj} + \Sigma, \tag{2.3}$$

where U_i represents the ith component of the velocity vector, P denotes pressure and T is the passive scalar. Σ represents a passive-scalar source term which is assumed to be steady and uniform or linear in each coordinate direction for the cases considered here. The density (ρ), the kinematic viscosity (ν) and the molecular kinematic diffusivity of the passive scalar (γ) are uniform throughout the flow field and constant in time. In the above equations, the Einstein summation convention is used and a comma followed by an index indicates differentiation with respect to the indexed spatial coordinate.

In the study of turbulence it is customary to divide the flow into mean and fluctuating fields. Substituting the decomposition

$$U_i = \overline{U}_i + u_i, \quad P = \bar{P} + p, \quad T = \bar{T} + \theta \tag{2.4}$$

into (2.1)–(2.3) and averaging yields the following equations governing the mean fields:

$$\overline{U}_{i,i} = 0, \tag{2.5}$$

$$\frac{\partial \overline{U}_i}{\partial t} + \overline{U}_j \overline{U}_{i,j} + (\overline{u_i u_j})_{,j} + \frac{1}{\rho}\bar{P}_{,i} = \nu \overline{U}_{i,jj}, \tag{2.6}$$

$$\frac{\partial \bar{T}}{\partial t} + \overline{U}_j \bar{T}_{,j} + (\overline{\theta u_j})_{,j} = \gamma \bar{T}_{,jj} + \Sigma. \tag{2.7}$$

It is readily apparent that closure of these equations requires the use of turbulence models for the Reynolds stress, $\overline{u_i u_j}$, and for the turbulent scalar flux, $\overline{\theta u_j}$. In this work it is assumed that closure models for the hydrodynamic field are available. The turbulent scalar flux is to be modelled in terms of given one-point properties of the hydrodynamic field, the local mean scalar gradient and the Prandtl number, ν/γ. Note that for homogeneous flows the Reynolds stress and the turbulent scalar flux exhibit no spatial gradients and the mean flow equations (2.5)–(2.7) are decoupled from the turbulence.

The trace of the Reynolds stress tensor, $q^2 = \overline{u_i u_i}$, represents twice the turbulent kinetic energy per unit mass. The rate of dissipation of turbulent kinetic energy in homogeneous flows is given by $\epsilon = \nu \overline{u_{i,j} u_{i,j}}$. The turbulence scales q^2 and ϵ can be used to generate turbulence length- and timescales and both are used in the model for the turbulent scalar flux derived in §3.

The governing equation for the turbulent scalar flux is

$$\frac{\partial \overline{\theta u_i}}{\partial t} = -\overline{u_i u_j}\bar{T}_{,j} - \overline{\theta u_j}\overline{U}_{i,j} + \frac{1}{\rho}\overline{p\theta}_{,i} - (\nu+\gamma)\overline{u_{i,j}\theta_{,j}} - \left(\overline{\theta u_i}\overline{U}_j + \overline{\theta u_i u_j} + \frac{1}{\rho}\overline{p\theta}\delta_{ij} - \nu\overline{\theta u_{i,j}} - \gamma\overline{u_i\theta_{,j}}\right)_{,j}. \tag{2.8}$$

The first two terms on the right of the above equation are production terms, one due to the interaction of Reynolds stresses and the mean scalar gradient and the other due to the scalar flux interacting with the mean velocity gradient. The pressure–scalar gradient covariance requires modelling and is found to reduce the scalar flux. The fourth term on the right of (2.8) is a dissipation term that is believed to be negligible at high Reynolds numbers (Launder 1978). The last term is zero in homogeneous flows.

2.2. *Homogeneous turbulent shear flow*

Shear flow turbulence can be homogeneous only if the mean shear rate is uniform in space. Here the mean flow direction is chosen to be the x_1-direction. The mean gradient or cross-stream direction is taken to be the x_2-direction and the spanwise direction is referred to as the x_3-direction. The mean velocities are thus

$$\overline{U}_1(x_2) = Sx_2, \quad \overline{U}_2 = 0, \quad \overline{U}_3 = 0, \tag{2.9}$$

where S denotes the constant and uniform mean shear rate $\partial\overline{U}_1/\partial x_2$. The fluctuating velocities are taken to be u_1, u_2 and u_3 in the x_1-, x_2- and x_3-directions, respectively.

In order to include all possible orientations of the mean passive-scalar gradient with respect to the mean shear, it is necessary to simulate cases with mean scalar gradients in three independent directions. Then, because the governing equation (2.3) for the passive scalar T is linear in T, the solution for any mean scalar gradient

(for a given hydrodynamic field) can be obtained by using superposition. These three independent directions are chosen to be the coordinate directions. Case 1 refers to a mean scalar gradient imposed in the streamwise or x_1-direction. Case 2 refers to the mean scalar gradient imposed in the cross-stream or x_2-direction and Case 3 consists of a mean scalar gradient imposed in the spanwise or x_3-direction. The scalar fluctuations for these three cases will be referred to as θ_1, θ_2 and θ_3, respectively.

For homogeneous turbulent shear flow in the above coordinate system, the mean field equations (2.5)–(2.7) become

$$\overline{U}_{1,1} = 0, \tag{2.10}$$

$$\frac{\partial \overline{U}_1}{\partial t} + \frac{1}{\rho}\bar{P}_{,1} = 0, \quad \bar{P}_{,2} = 0, \quad \bar{P}_{,3} = 0, \tag{2.11}$$

$$\frac{\partial \bar{T}}{\partial t} + (Sx_2)\,\bar{T}_{,1} = \Sigma. \tag{2.12}$$

As noted before, in homogeneous flows the mean velocity and scalar fields are unaffected by the turbulence. To maintain a steady mean velocity field, it is necessary to have a uniform mean pressure field. The mean scalar field is steady if $\Sigma = 0$ unless the mean scalar gradient has a component in the streamwise direction. In this case, for the mean scalar field to be steady $\Sigma = (Sx_2)\,\bar{T}_{,1}$. The mean shear creates a mean scalar gradient component in the x_2-direction from an imposed mean scalar gradient component in the x_1-direction because the mean shear moves fluid at large x_2 faster than fluid at small x_2. The above source term will permit a steady mean scalar gradient with only an x_1-dependence by generating the scalar quantity at a rate that exactly cancels the tendency of the mean shear to produce a mean scalar gradient component in the x_2-direction. Because this source term is steady, it does not appear in the fluctuating scalar equations.

The numerical method used to solve the governing equations for the homogeneous shear flow is that of Rogallo (1977, 1981) and has been described in detail in his work and by Lee & Reynolds (1985). Fourier-pseudospectral methods (see Orszag & Patterson 1972) are used to represent the spatial variation of flow variables and their spatial derivatives. Periodic boundary conditions are implemented in all three coordinate directions by employing a transformation in which the computational grid deforms in accordance with the mean flow. To allow the simulation to progress for a substantial time, it is necessary to remesh the grid at regular intervals. The fields at even integral values of St are on an orthogonal mesh and are saved for analysis. In order to avoid costly convolution sums in Fourier space, nonlinear velocity products are computed in physical space. Aliasing errors that occur when velocity products are computed in this fashion are removed by a combination of truncation and random phase shift methods. The time advancement is accomplished by a second-order Runge–Kutta method. Initial conditions for all the simulations consist of randomly generated isotropic fields with prescribed initial energy and scalar spectra.

The ability of the computational grid to resolve the relevant turbulent scales of motion must be checked as the simulation progresses. Problems can develop at both large and small scales. Since large-eddy lengthscales in homogeneous shear flow grow in time, it is important that an adequate sample of large eddies exists in the computational box at all times. When this condition is no longer satisfied (as indicated by an inability to capture all the turbulent kinetic energy at low wavenumbers or by a two-point correlation function that does not decrease to zero

	C128R simulation	C128S simulation	C128U simulation	C128V simulation	C128W simulation	C128X simulation
N_x	128	128	128	128	128	128
N_y	128	128	128	128	128	128
N_z	128	128	128	128	128	128
Δx	0.07792	0.07792	0.07792	0.07792	0.07792	0.07792
Δy	0.03896	0.03896	0.03896	0.03896	0.03896	0.03896
Δz	0.03896	0.03896	0.03896	0.03896	0.03896	0.03896
S	28.284	28.284	28.284	28.284	56.568	14.142
ν	0.010	0.010	0.010	0.020	0.020	0.005
q_0^2	31.96	31.96	31.96	31.96	31.96	31.96
S_θ	2.5	2.5	2.5	2.5	2.5	2.5
Pr	1.0	0.2	0.7	2.0	2.0	0.7
$\overline{\theta^2}_0$	31.96	31.96	31.96	31.96	31.96	31.96

TABLE 1. Simulation parameters. Pulse initial energy and scalar spectra with $\frac{1}{2}E_{ii}(k) = 1$ and $\frac{1}{2}E_\theta(k) = 1$ between $k = 16$ and $k = 32$

within the computational box), the numerical simulations no longer represent physical turbulence. It is also necessary to ensure that the small scales contributing to the dissipation of turbulent kinetic energy are well-resolved by the computational grid. This will automatically ensure that the small-scale contribution to the turbulent kinetic energy is adequately captured. The smallest eddies in the flow (as indicated by the Kolmogorov scale) become smaller because the rate of dissipation of turbulent kinetic energy increases for large time, St. Thus the grid spacing will eventually become inadequate to capture the small scales of motion. For a limited number of grid points it is possible to resolve only a limited range of scales, and this limits the numerical simulations to low Reynolds numbers. Ideally, the computation runs out of computational grid at both the large- and small-scales at the same time, allowing the widest range of scales (and therefore largest Reynolds number) on a given grid. The two-point scalar correlations, the scalar spectra and the scalar dissipation spectra were also monitored to ensure that all essential scales of passive-scalar motion were captured by the computational grid.

All simulations were done on the CRAY X-MP at the NASA-Ames Research Center. The $128 \times 128 \times 128$ grid simulations used here took about 20 s per time-step to generate the hydrodynamic field and an additional 25 s per time-step to simulate the three passive-scalar fields resulting from mean scalar gradients in each of the coordinate directions. The different simulations ran between 900 and 1400 time-steps before the computational mesh became inadequate to resolve the turbulence.

The parameters for the simulations are given in table 1. The C128R, C128S and C128U simulations all used the (recalculated) hydrodynamic field from the high-Reynolds number simulation of Rogers & Moin (1987) with Prandtl numbers $Pr =$ 1.0, 0.2 and 0.7, respectively. Prandtl numbers greater than 1.0 could not be simulated with this hydrodynamic field because the relatively weak scalar diffusivity for such cases allows very small scalar motions (compared to the smallest scales of motion of the velocity field) to exist without adequate computational grid for them to be resolved.† For this reason, in order to simulate large-Prandtl-number scalar flows, the Reynolds number must be reduced to provide extra resolution at the high-wavenumber end of the spectrum. Maintaining a high enough Reynolds number for

† Because of the pressure term in (2.2) the small-scale hydrodynamic field is better resolved than the small-scale scalar field at $Pr = 1.0$.

a realistic turbulent flow that compares well to experiment puts a severe limitation on the Prandtl number and it was not possible to generate satisfactory fields for $Pr > 2$. The C128V and C128W simulations resolve a $Pr = 2.0$ passive scalar by reducing the Reynolds number. The C128X simulation provides another $Pr = 0.7$ case that can be compared to the experimental work.

The initial scalar spectrum for these simulations was a rectangular pulse over the same range of wavenumbers as the initial energy spectrum. Other initial scalar spectra were not used, but Shirani, Ferziger & Reynolds (1981) have shown that in homogeneous turbulent shear flow the scalar field rapidly adjusts itself to the velocity field and the scalar spectrum becomes independent of its initial form.

A comparison of statistics of the hydrodynamic field to those observed experimentally by Tavoularis & Corrsin (1981) is made in Rogers & Moin (1987) and a more thorough analysis, including a comparison of the passive-scalar results with data from both Tavoularis & Corrsin (1981) and Tavoularis & Corrsin (1985), is presented in Rogers, Moin & Reynolds (1986). In general the agreement is quite good despite the substantial difference in Reynolds number between the simulations and the experiments. A brief description of the passive-scalar field development is described in the remainder of this section.

The solution of the passive-scalar equations involves specifying a mean scalar gradient and a molecular scalar diffusivity, γ. The mean scalar gradient in all the simulations has the same magnitude, denoted by S_θ, in each of the three coordinate directions. The time development of the r.m.s. values of the scalar fluctuations, $\theta' = (\overline{\theta^2})^{\frac{1}{2}}$, exhibits growth similar to that observed in the experimental work. In agreement with Tavoularis & Corrsin (1985), θ'_3 is slightly larger than θ'_2. No experimental data are available for Case 1, but all simulations show θ'_1 to be much larger than θ'_2 or θ'_3. The dissipation of scalar fluctuation intensity, $\overline{\theta^2}$, is given by $2\chi = 2\gamma\overline{\theta_{,j}\theta_{,j}}$. There is much uncertainty about the value of χ in the experiments but the qualitative behaviour and approximate magnitude of statistics involving χ are in good agreement with the simulated results.

The quantities S_θ, θ', χ and γ are analogous to the quantities S, q, ϵ and ν characterizing the behaviour of the velocity field. From these scales a lengthscale, θ'/S_θ, and a timescale, $(\theta')^2/\chi$, can be formed. The ratios of the analogous scales of the velocity field to these two scales yield two dimensionless parameters:

$$B = \frac{(q/S)}{(\theta'/S_\theta)}, \quad R = \frac{(q^2/\epsilon)}{((\theta')^2/\chi)}. \tag{2.13}$$

B represents the relative strength of the fluctuating velocity field compared to the fluctuating scalar field and R represents the ratio of the hydrodynamic turbulence timescale to the scalar turbulence timescale. These two parameters rapidly reach a roughly constant value in the simulations (see figure 1), the value of which depends on the Prandtl number and the orientation of the mean scalar gradient but appears to be relatively insensitive to other parameters. Thus both length- and timescales of the passive-scalar field quickly adjust themselves in accordance with those of the velocity field.

In agreement with the experimental results of Tavoularis & Corrsin (1981) the scalar fluctuations are distributed according to a Gaussian distribution and the joint velocity–scalar distributions are very close to joint normal. The skewness of the velocity and scalar gradient fluctuations is also in good agreement with experiment.

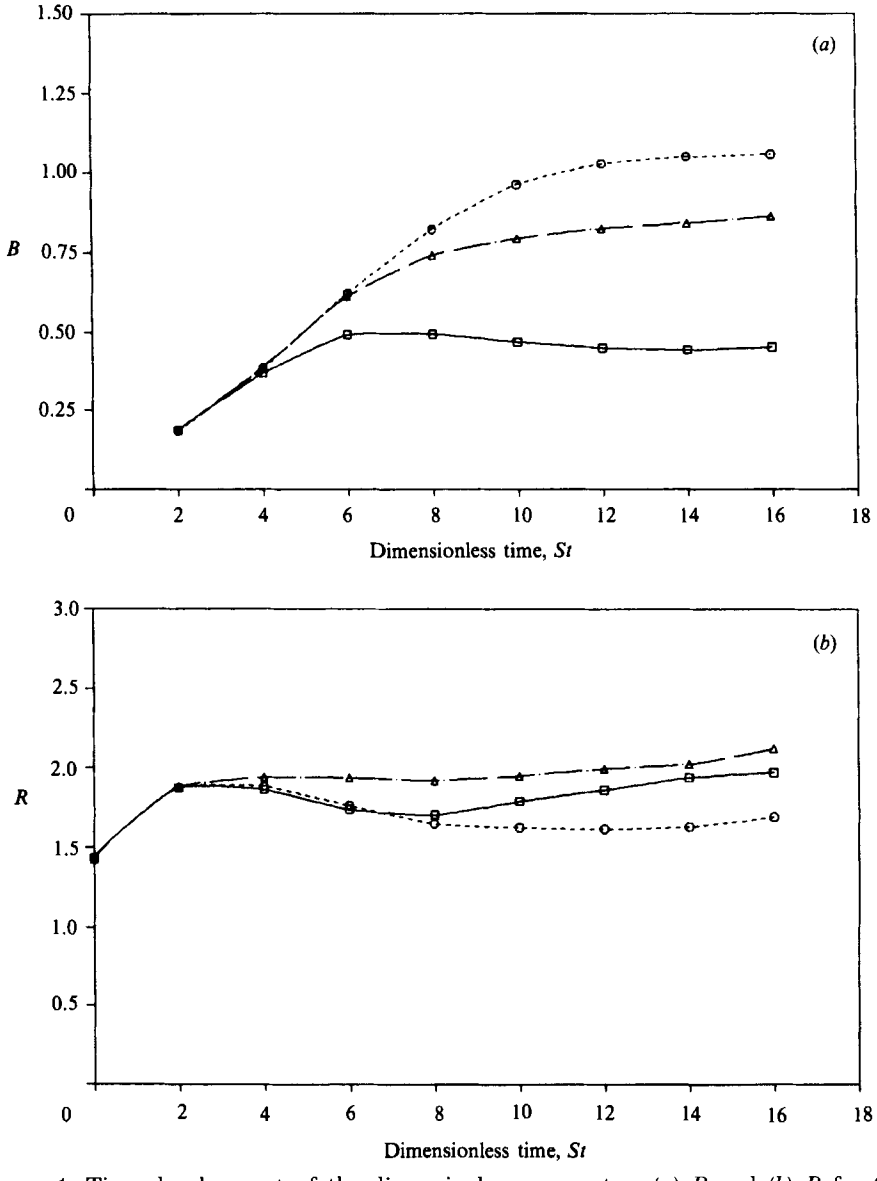

FIGURE 1. Time development of the dimensionless parameters (*a*) B and (*b*) R for the C128U simulation. □, ○, △, Cases 1, 2, 3, respectively.

2.3. *Fully developed turbulent channel flow*

The direct numerical simulations of fully developed turbulent channel flow are taken from Kim, Moin & Moser (1987) on a $128 \times 129 \times 128$ grid. The Reynolds number based on the channel half-width, δ, and the wall-friction velocity, u_τ, is 180. Pseudospectral methods are used to represent the spatial variation of flow variables and their spatial derivatives. Periodic boundary conditions are implemented in the streamwise, x_1-, and the spanwise, x_3-, directions permitting the use of Fourier series to describe the velocity in these two directions. Chebyshev polynomials are used for the mean gradient or x_2-direction to accommodate no-slip boundary conditions.

Aliasing errors are removed by expanding the number of collocation points by a factor of $\frac{3}{2}$ before transforming into the physical space. Time advancement is accomplished by the Crank–Nicolson method for the viscous terms and the Adams–Bashforth method for the nonlinear terms. The simulations were run until statistical stationarity was reached and then turbulent statistics were gathered by averaging over (x_1, x_3)-planes and 20 realizations.

Two different passive-scalar fields were simulated (Kim & Moin 1987). The first corresponds to the case where a passive scalar is added at the lower wall and removed from the upper wall at the same rate (referred to as WT or wall transfer case) and the second represents a case where the passive scalar is generated internally by a uniform steady source term and removed at both walls (referred to as IS or internal source case). Both of these passive-scalar fields reach a statistically steady state after the hydrodynamic field is fully developed. Each of these cases was run at Prandtl numbers of 0.10, 0.71 and 2.00. The computed results were in good agreement with existing experimental results.

3. Model development from homogeneous shear flow data

In a homogeneous flow there can be no spatial gradients of the turbulent scalar flux but it can assume uniform non-zero values. A positive correlation between θ and u_i results in a positive flux and vice versa. When the scalar is temperature, this corresponds to hot fluid moving in the positive direction or cold fluid moving in the negative direction.

Because the flux is based on the behaviour of a passive scalar that does not affect the velocity field, it is reasonable to expect that it would be possible to model this quantity based solely on characteristics of the velocity field, the imposed uniform mean scalar gradient and the Prandtl number. Sreenivasan, Tavoularis & Corrsin (1981) have shown that gradient-transport-type models work well for predicting the scalar flux in homogeneous flows. The simplest and most commonly used gradient transport model is

$$\overline{\theta u_i} = -\gamma_T \overline{T}_{,i}. \tag{3.1}$$

This model is analogous to the Fourier constitutive equation for heat conduction and assumes that the scalar flux is down the mean scalar gradient. The constant of proportionality, γ_T, is referred to as the turbulent eddy diffusivity.

The simulations and the experimental work both show the model of equation (3.1) to be inadequate. The scalar flux in homogeneous turbulent shear flow is not, in general, aligned with the mean scalar gradient (see figure 2). Additionally, the magnitude of the flux component down the gradient varies substantially, depending on the direction of the imposed mean scalar gradient. Figure 3 illustrates the time development of the turbulent Prandtl number based on the magnitude of the flux component in the mean scalar gradient direction, $Pr_T = (-\overline{u_1 u_2}/S)/\gamma_T$. For Case 2 (mean scalar gradient parallel to the mean shear) $Pr_T \approx 0.85$ which is in good agreement with typical values found in the turbulent boundary layer (see Kays & Crawford 1980) and in other inhomogeneous flows. The experimental values in homogeneous shear flow are slightly higher than the simulated results. For Case 1 and Case 3, however, the turbulent Prandtl number is far from one and using this assumption for these cases would be grossly in error. The physical relevance of Pr_T is thus questionable because this parameter depends strongly on the orientation of the mean scalar gradient with respect to the mean shear.

Because (3.1) cannot represent the behaviour of the scalar flux using a scalar

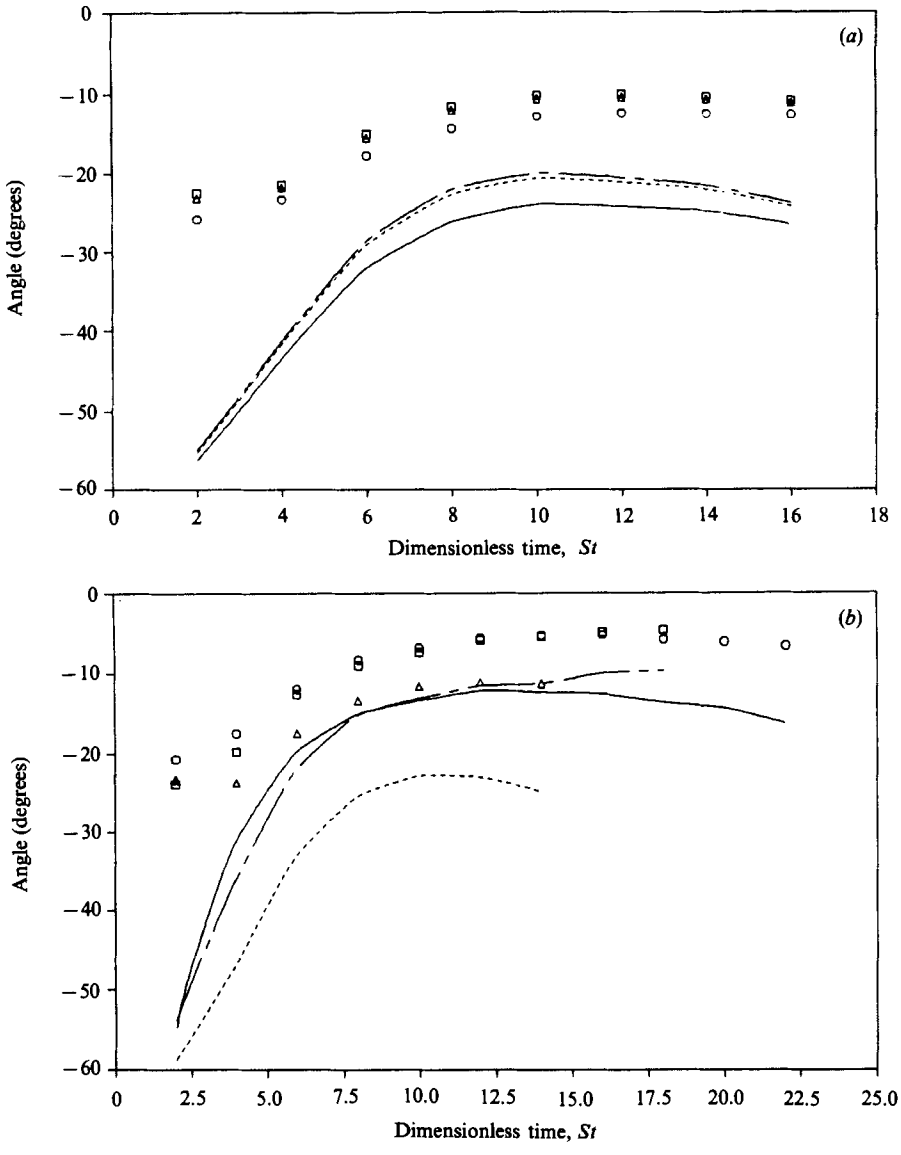

FIGURE 2. Time development of $\alpha_f = \tan^{-1}(\overline{\theta u_2}/\overline{\theta u_1})$, the turbulent scalar flux direction. (*a*) □, ○, △, Case 1: C128R, C128S, C128U; — — —, ——, – – – –, Case 2: C128R, C128S, C128U; (*b*) □, ○, △, Case 1: C128V, C128W, C128X; — — —, ——, – – – –, Case 2; C128V, C128W, C128X. Note Case 3 flux is down the mean gradient, and down-the-mean-gradient directions for Cases 1 and 2 correspond to 0° and −90°, respectively.

turbulent eddy diffusivity, it becomes necessary to implement a tensor eddy diffusivity as suggested by Batchelor (1949). This yields

$$\overline{\theta u_i} = -D_{ij}\bar{T}_{,j}, \tag{3.2}$$

where D_{ij} is the turbulent eddy diffusivity tensor. Because the flux vector is not aligned with the mean scalar gradient, D_{ij} is not a diagonal tensor. Since each column is derived from a different physical experiment (it is necessary to simulate three independent mean scalar gradients to determine all nine components of D_{ij}), there

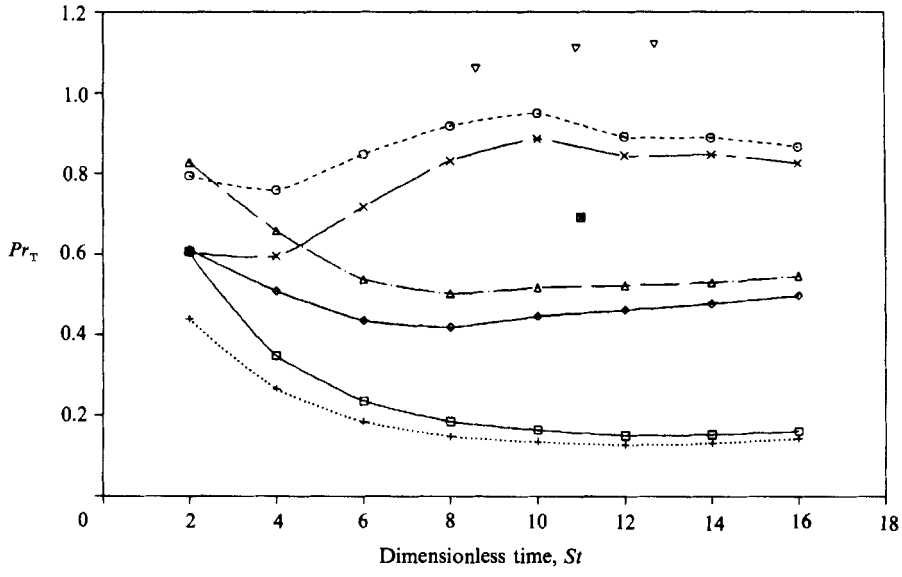

FIGURE 3. Time development of the turbulent Prandtl number, Pr_T, for the C128S and C128U simulations. □, ○, △, Cases 1, 2, 3, C128S simulation; +, ×, ◇, Cases 1, 2, 3, C128U simulation; ▽, ⊠, Cases 2, 3, Tavoularis & Corrsin (1981), Tavoularis & Corrsin (1985).

is no physical reason for D_{ij} to be symmetric and indeed both experimental and numerical results show that D_{ij} is not symmetric. For the coordinate system (2.9), flow symmetry implies

$$D_{13} = D_{23} = D_{31} = D_{32} = 0, \tag{3.3}$$

a result that is confirmed by the computations. Thus the flux resulting from a spanwise mean scalar gradient is aligned with it. Fluxes resulting from a mean scalar gradient imposed in the (x_1, x_2)-plane lie in that plane but are not aligned with the mean scalar gradient. In fact, as can be seen in figure 2, the flux direction is inclined at about 15° below the streamwise coordinate direction for both Cases 1 and 2. The turbulence thus dominates simple down-the-gradient transport.

The existence of hairpin vortices in homogeneous turbulent shear flow (Rogers & Moin 1987) can be used to explain the nature of the turbulent scalar flux. The inclined coherent hairpin-like vortex structures tend to pump the scalar between their legs. If this provided the dominant mechanism for turbulent scalar transport then the turbulent scalar flux direction should depend on the coherent vortex structure orientation and not on the orientation of the mean scalar gradient across the structure. Figure 2 provides evidence that this is to a large extent the case. In addition, the scalar fields of Cases 1 and 2 are expected to be well correlated because for these two cases the hairpin vortices create the same regions of high scalar intensity. In all the numerical simulations the initially uncorrelated scalar fluctuations θ_1 and θ_2 became over 75% correlated as the scalar fields developed. Further indication of the alignment of the scalar flux with characteristic directions of the hydrodynamic field is particularly evident for Case 2. Figure 4 compares the time development of the principal angle of the Reynolds stress tensor,

$$\alpha_b = \tfrac{1}{2}\tan^{-1}(2\overline{u_1 u_2}/(\overline{u_1^2} - \overline{u_2^2})),$$

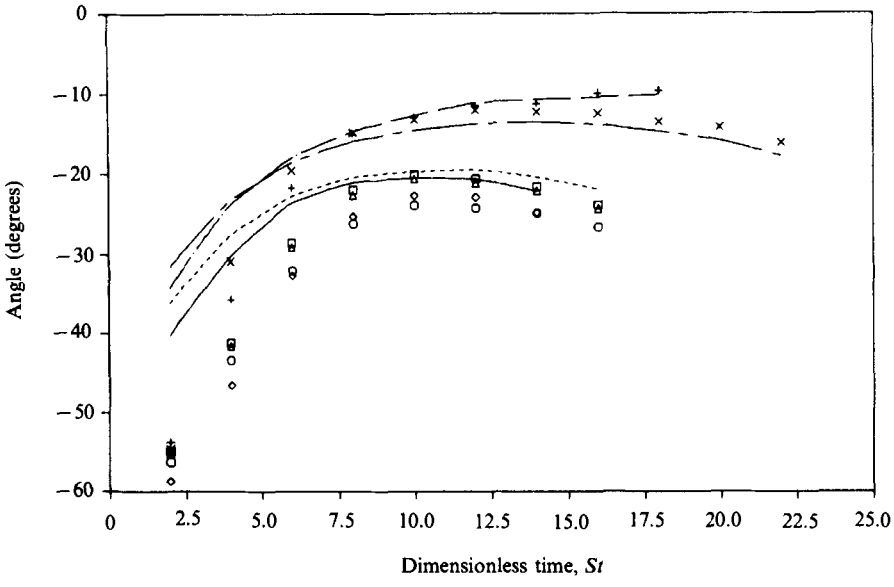

FIGURE 4. Comparison of the turbulent scalar flux direction, α_f, for Case 2 with α_b. □, α_f, C128R simulation; ○, α_f, C128S simulation; △, α_f, C128U simulation; +, α_f, C128V simulation; ×, α_f, C128W simulation; ◇, α_f, C128X simulation; – – –, α_b, C128R, C128S, C128U simulations; — · —, α_b, C128V simulation; — — —, α_b, C128W simulation; ——, α_b, C128X simulation.

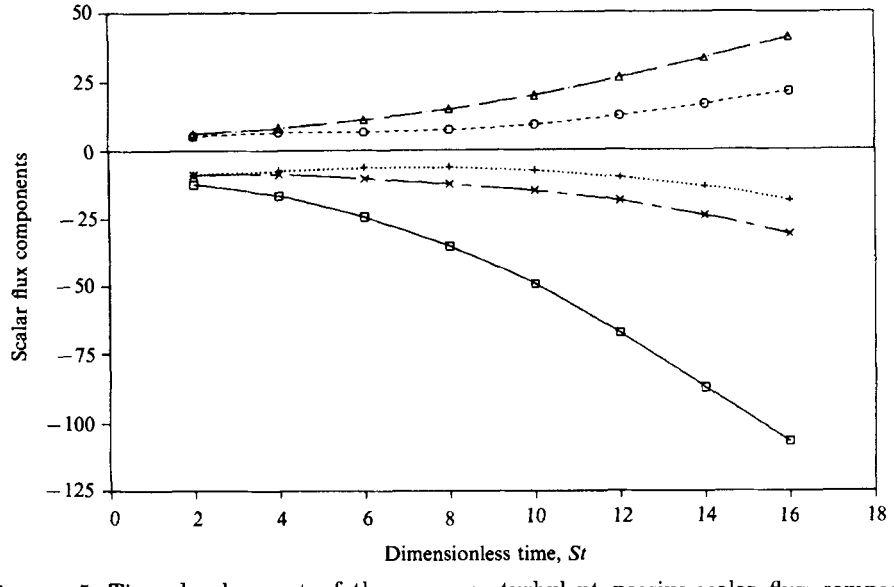

FIGURE 5. Time development of the non-zero turbulent passive-scalar flux components, $\overline{\theta_\alpha u_i}$ (normalized by γS_θ), for the C128U simulation. □, $\overline{\theta_1 u_1}$; ○, $\overline{\theta_1 u_2}$; △, $\overline{\theta_2 u_1}$; +, $\overline{\theta_2 u_2}$; ×, $\overline{\theta_3 u_3}$.

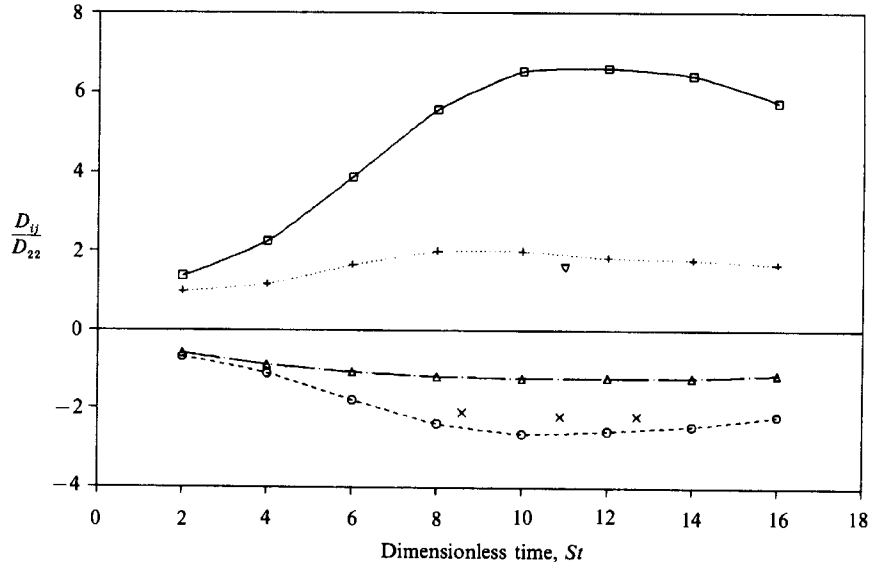

FIGURE 6. Time development of the turbulent eddy diffusivity tensor, D_{ij}/D_{22} for the C128U simulation. □, D_{11}/D_{22}; ○, D_{12}/D_{22}; △, D_{21}/D_{22}; +, D_{33}/D_{22}; ×, D_{12}/D_{22} (Tavoularis & Corrsin 1981); ▽, D_{33}/D_{22} (Tavoularis & Corrsin, 1985).

with that of the inclination angle of the turbulent scalar flux,

$$\alpha_f = \tan^{-1}(\overline{\theta u_2}/\overline{\theta u_1}).$$

It is readily apparent that the flux rapidly aligns itself with the principal axes of the Reynolds stress tensor for this case, particularly when Pr is greater than 0.2. It should be noted that since α_f for Case 1 is close to that of Case 2 (figure 2) α_b also gives a rough indication of the flux inclination angle for Case 1.†

Figure 5 shows the time development of the non-zero turbulent scalar flux components for each imposed mean scalar gradient from the C128U simulation. Other simulations behave in a similar fashion. Because the magnitude of the scalar gradient is the same for each case, the components of D_{ij} behave in the same manner as the fluxes. The components of D_{ij} normalized by D_{22}, the conventional scalar eddy diffusivity, for the C128U simulation are shown in figure 6. The other simulation results are qualitatively similar. The simulation is in good agreement with the experimental results of Tavoularis & Corrsin (1981, 1985) despite significant Reynolds-number differences. No experimental data are available for the case of a mean streamwise scalar gradient.

The governing equation for the turbulent scalar flux in homogeneous flows is

$$\left.\begin{aligned} \frac{\partial \overline{\theta u_i}}{\partial t} &= -\overline{u_i u_j}\,\overline{T}_{,j} - \overline{\theta u_j}\,\overline{U}_{i,j} + \psi_i, && (3.4a)\\ \psi_i &= \frac{1}{\rho}\overline{p\theta}_{,i} - (\nu+\gamma)\,\overline{u_{i,j}\theta_{,j}}. && (3.4b) \end{aligned}\right\}$$

† This approximate equality of α_b and α_f was found to hold in the fully developed turbulent channel flow simulation results as well. For the IS case agreement was good throughout the channel, particularly for $Pr = 0.71$ and $Pr = 2.0$. The equality does break down in the central region of the channel for the WT case where the flux is directed vertically yet $\overline{u_1 u_2}$ and α_b approach zero. In the lower half of the channel, however, the agreement is excellent for $Pr = 0.71$ and $Pr = 2.0$ and within about 10° for $Pr = 0.1$.

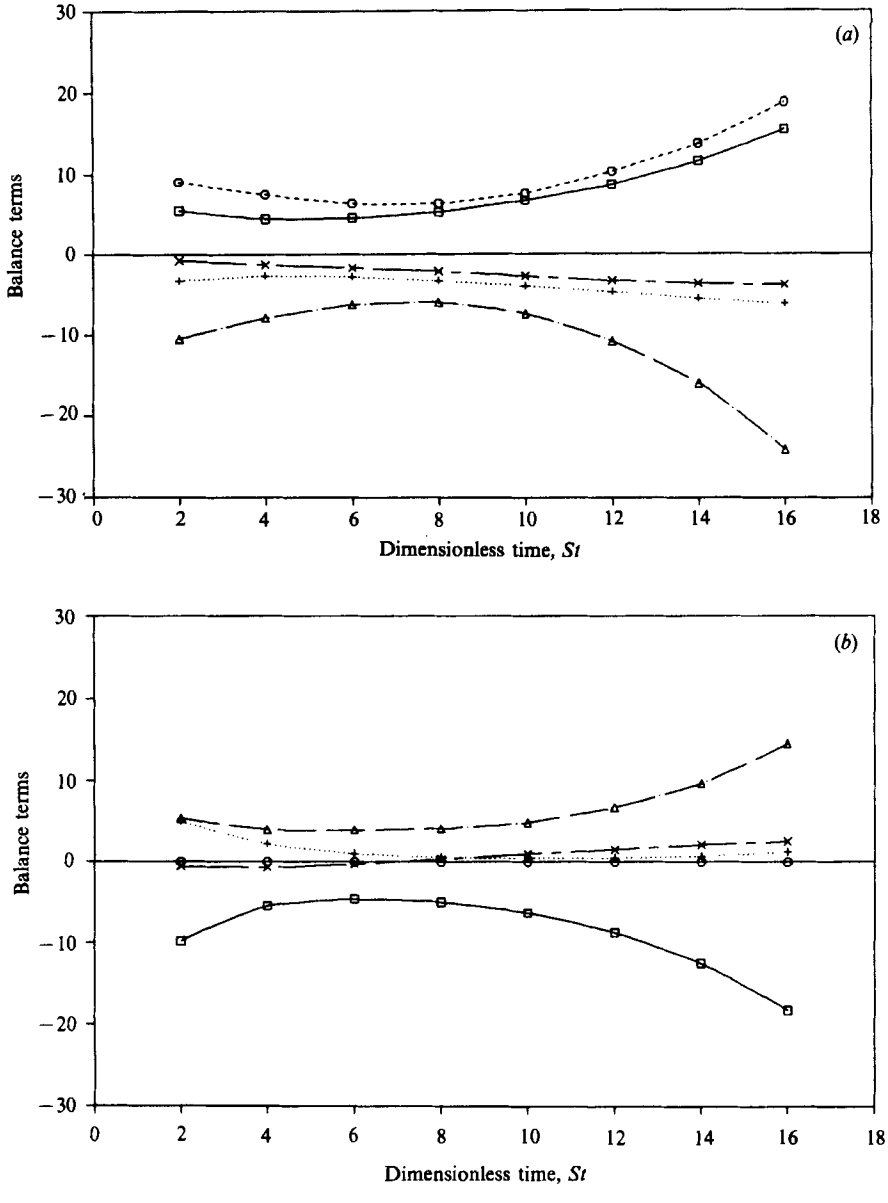

FIGURE 7. Time development of the scalar flux balance (normalized by $\gamma S_g S$) for Case 2 of the C128U simulation. (*a*) $\overline{\theta u_1}$ balance ($i = 1$); (*b*) $\overline{\theta u_2}$ balance ($i = 2$). □, $-\overline{u_i u_2}\,\overline{T}_{,2}$; ○, $-\overline{\theta u_2}\,\overline{U}_{i,2}$; △, $-(1/\rho)\overline{\theta p}_{,i}$; +, $-(\nu+\gamma)\overline{u_{i,j}\theta_{,j}}$; ×, $-\partial\overline{\theta u_i}/\partial t$.

The first two terms on the right-hand side of (3.4*a*) are production terms that do not have to be modelled. The terms in ψ_i must be modelled (although local isotropy of small scales implies that the dissipation term is small for large Reynolds numbers). The behaviour of these terms has been studied by examining many simulated flow fields. Figure 7 shows the balance of the terms in (3.4*a*, *b*) for Case 2 of the C128U simulation. The behaviour of the individual terms in the scalar flux equations will now be examined.

The term $\partial\overline{\theta u_i}/\partial t$ is generally smaller than the terms on the right-hand side of the

equation but is not zero. However, the correlation coefficient $\overline{\theta u_i}/(\theta' q)$ does appear to reach a constant value when the flow becomes developed, implying that

$$\frac{\partial \overline{\theta u_i}/(\theta' q)}{\partial t} \approx 0. \tag{3.5}$$

Differentiation together with the governing equations for the turbulent kinetic energy and the scalar fluctuation intensity then yields

$$\frac{\partial \overline{\theta u_i}}{\partial t} \approx \frac{\overline{\theta u_i}}{q^2}(\mathscr{P}-\epsilon)+\frac{\overline{\theta u_i}}{\overline{\theta^2}}(\mathscr{P}_\theta-\chi) = \text{scalar} \times \overline{\theta u_i}, \tag{3.6}$$

where $\mathscr{P} = -\overline{u_1 u_2}S$ and $\mathscr{P}_\theta = -\overline{\theta u_j}\,\overline{T}_{,j}$ denote the production rates of $\frac{1}{2}q^2$ and $\frac{1}{2}\overline{\theta^2}$, respectively. This indicates that the change in θu_i is exactly aligned with θu_i itself when the correlation coefficient derivative in (3.5) is exactly zero. Direct examination of the scalar flux direction (figure 2) shows that it is indeed approximately constant for the developed shear fields.

The 'dissipation' term in (3.4*b*), $-(\nu+\gamma)\overline{u_{i,j}\theta_{,j}}$, is typically small for the high-Reynolds-number fields at large St. The balance for $\overline{\theta u_2}$ from Case 1 shows that this so-called dissipation term is negative at large St and thus acts as a production term for this case. The pressure term in (3.4*b*) always causes flux dissipation and is roughly aligned opposite to the flux direction. The sum ψ_i is even more closely aligned opposite to the flux direction. Lumley (1978) has defined $\phi^\theta_{ij} = -\psi_i(q^2/\epsilon)/\overline{\theta u_j}$ in studying the decay of the scalar flux in a flow returning to isotropy. Thus, in this notation, the simulation results indicate that $\phi^\theta_{ij} \approx \phi^\theta \delta_{ij}$ in homogeneous turbulent shear flow. This result has been assumed by Zeman & Lumley (1979) and Newman, Launder & Lumley (1981) who take $\phi^\theta = 7.5$ and 6.6, respectively. Shih & Lumley (1986) take ϕ^θ_{ij} to be isotropic but model ϕ^θ in terms of the timescale ratio, R, instead of assuming it to be constant.

It thus seems reasonable that both ψ_i and the time change of the scalar flux can be replaced by a multiple of the scalar flux vector, yielding

$$0 = -\overline{u_i u_j}\,\overline{T}_{,j} - \overline{\theta u_j}\,\overline{U}_{i,j} - C_D\frac{1}{\tau}\overline{\theta u_i}, \tag{3.7}$$

where C_D is a dimensionless coefficient and τ is an appropriate timescale. (Note that C_D and the tensor O_{ij} defined below are of opposite sign to those used in Rogers *et al.* 1986). Equation (3.7) implies that the sum of the two scalar flux production terms is aligned with the scalar flux vector, an easier assumption to check in practice than the alignment of the modelled terms with the flux vector. The governing equation has now been reduced to an algebraic equation for $\overline{\theta u_i}$ and can be solved. Defining a tensor O_{ij},

$$O_{ij} = \frac{C_D}{\tau}\delta_{ij} + \overline{U}_{i,j}, \tag{3.8}$$

leads to

$$O_{ij}\overline{\theta u_j} = -\overline{u_i u_j}\,\overline{T}_{,j}. \tag{3.9}$$

Inversion of the 3×3 matrix O_{ij} then yields

$$\overline{\theta u_i} = -O^{-1}_{in}\overline{u_n u_j}\frac{\partial \overline{T}}{\partial x_j} = -(\tfrac{1}{2}O^{-1}\epsilon_{pki}\epsilon_{lmn}O_{lp}O_{mk}\overline{u_n u_j})\frac{\partial \overline{T}}{\partial x_j}, \tag{3.10}$$

where O^{-1} is the reciprocal of the determinant of O_{ij}. Note that the gradient transport form of this model has been derived directly from the governing equation for the

passive-scalar flux with the assumption that the sum of the modelled terms can be represented by a vector aligned with $\overline{\theta u_i}$. The definition of D_{ij} (equation (3.2)) finally results in (the superscript M indicates model prediction)

$$D_{ij}^{\mathrm{M}} = \tfrac{1}{2} O^{-1} \epsilon_{pki}\, \epsilon_{lmn}\, O_{lp}\, O_{mk}\, \overline{u_n u_j}, \tag{3.11}$$

or, on a component basis,

$$D_{11}^{\mathrm{M}} = \frac{\tau}{C_D}\overline{u_1^2} + S\tau \frac{\tau}{C_D^2}(-\overline{u_1 u_2}), \tag{3.12}$$

$$D_{12}^{\mathrm{M}} = -\frac{\tau}{C_D}(-\overline{u_1 u_2}) - S\tau \frac{\tau}{C_D^2}\overline{u_2^2}, \tag{3.13}$$

$$D_{21}^{\mathrm{M}} = -\frac{\tau}{C_D}(-\overline{u_1 u_2}), \tag{3.14}$$

$$D_{22}^{\mathrm{M}} = \frac{\tau}{C_D}\overline{u_2^2}, \tag{3.15}$$

$$D_{33}^{\mathrm{M}} = \frac{\tau}{C_D}\overline{u_3^2}. \tag{3.16}$$

For $S\tau/C_D \gg 1$ the matrix O_{ij} becomes stiff. This does not create any difficulties for the model because the inversion is done analytically. From (3.12)–(3.16) it can be seen that under this condition the streamwise fluxes will dominate. This is expected because the shear production term in the scalar flux balance equation (3.4*a*) contributes only to the streamwise flux component. For the simulations considered here $S\tau/C_D < 2.5$ because the turbulence timescale τ adjusts itself to the value of S such that $S\tau$ reaches a constant that is typically only slightly larger than C_D. Other possible realizability restrictions, such as the condition that the scalar-flux correlation coefficients remain less than one in absolute value, cannot be investigated without a model for the scalar fluctuation intensity, $\overline{\theta^2}$.

This model has only one dimensionless coefficient and generates D_{ij} from a multiplication of a tensor containing the mean shear information and the Reynolds stress tensor. This formulation resembles the original governing equation in that the mean shear appears explicitly only in the D_{1j} elements, consistent with the fact that the mean shear directly contributes only to the streamwise flux component in the scalar flux governing equation.

Gibson & Launder (1976) have used (3.5) (and assumed that the spatial gradients of the same correlation coefficient are zero for inhomogeneous flows) to develop an algebraic stress model for the passive-scalar flux vector. However they model ψ_i as

$$\psi_i = -c_{1T}\left(\frac{2}{\tau}\right)\overline{\theta u_i} + c_{2T}\,\overline{\theta u_j}\,\overline{U}_{i,j}. \tag{3.17}$$

This form results from (3.4*b*) by neglecting the dissipation term and modelling the 'slow' and 'rapid' parts of the pressure term by the first and second terms on the right-hand side of (3.17), respectively. When $c_{2T} \neq 0$ (Gibson & Launder 1976 use 0.50), this implies that ψ_i is not aligned with $\overline{\theta u_i}$ and leads to different expressions for D_{ij}^{M}. The simulation results indicate that splitting the pressure term into rapid and slow parts is not a good idea. The 'slow' pressure term and the sum of the 'slow' pressure term and the dissipation term are not as closely aligned with the scalar flux

as either the total pressure term or the sum of the total pressure and dissipation terms.

Tavoularis & Corrsin (1985) used 'mostly material coordinates' to arrive at expressions that appear somewhat similar to (3.12)–(3.16). If all their timescales T_{ij} are taken as equal, with a value of τ/C_D (although their estimates vary by a factor of four), their expression (21) would be the same as the above estimates for the diagonal entries of D_{ij} except for the fact that the sign of the second term for D_{11} is opposite to that of (3.12). Thus their value of D_{11} is a difference of two terms (implying D_{11} could be negative) as opposed to the estimate given here which is the sum of two positive terms. Their estimates of the off-diagonal terms are interchanged compared to (3.13) and (3.14) with the mean shear affecting the D_{21} rather than the D_{12} component. This is contrary to what is expected from the governing equation (3.4a). In addition, the sign of the mean shear term is opposite that of the second term in (3.13) implying D_{21} could be positive. Both D_{21} and D_{12} must be negative (or, more exactly, opposite in sign to S) according to (3.13) and (3.14).

There are five non-zero components of D_{ij} and only one free coefficient C_D. The averaging method employed to determine C_D consists of averaging the five C_D estimates obtained from (3.7). This is not the same as the average of the five C_D estimates determined by (3.12)–(3.16) but is close for the simulation data considered here (the two estimates would be exactly the same if there were no scatter in the five C_D estimates).

The choice $\tau = q^2/\epsilon$ generates values of C_D that grow monotonically in time and are easiest to model as described below. This choice is consistent with Lumley (1978) and the more recent work in scalar-field modelling cited above. However, the coefficient C_D is not the same as the ϕ^θ used by turbulence modellers because the time change of the scalar flux is included in C_D and not in ϕ^θ.

The behaviour of C_D for all six scalar simulations in homogeneous shear flow is shown in figure 8 (simulation results are indicated by the symbols). Launder (1978) presents data from a variety of experimenters based on (3.15) that yield C_D ranging from 5 to 19.4. This coefficient can be modelled in terms of the available dimensionless scalar parameters, including $Re_T = q^4/(\epsilon\nu)$, Sq^2/ϵ, Pr and St, and the Reynolds stress tensor invariants. The invariants were eliminated for simplicity and St was not considered because the turbulence growth with St is affected by the initial conditions. Shih & Lumley (1986) model ϕ^θ in terms of the timescale ratio, $R = (q^2/\epsilon)/(\overline{\theta^2}/\chi)$. This necessitates solving additional equations for $\overline{\theta^2}$ and χ, and is done to incorporate the effects of different initial scalar conditions in the return-to-isotropy problem. In the homogeneous turbulent shear flow simulations R rapidly approaches a constant value whereas C_D continually increases and it is therefore clear that C_D must be primarily dependent on some other parameter. In addition, not basing C_D on R avoids violating the linearity and independence principles set forth by Pope (1983).

Because the C128R, C128S and C128U simulations have the same velocity field, the Prandtl (or Péclet, $Pe = Re_T Pr$) number effect on the model coefficient can be isolated. It was found by trial and error that a function of the form

$$a_0\left(1+\frac{a_2}{Pe}\right)^{a_3} \tag{3.18}$$

could describe this behaviour. This function approaches a_0 for large Pe; and, depending on the sign of a_3, approaches infinity or zero when Pe tends to zero. The fact that large-scale turbulence statistics reach a value independent of Pe for

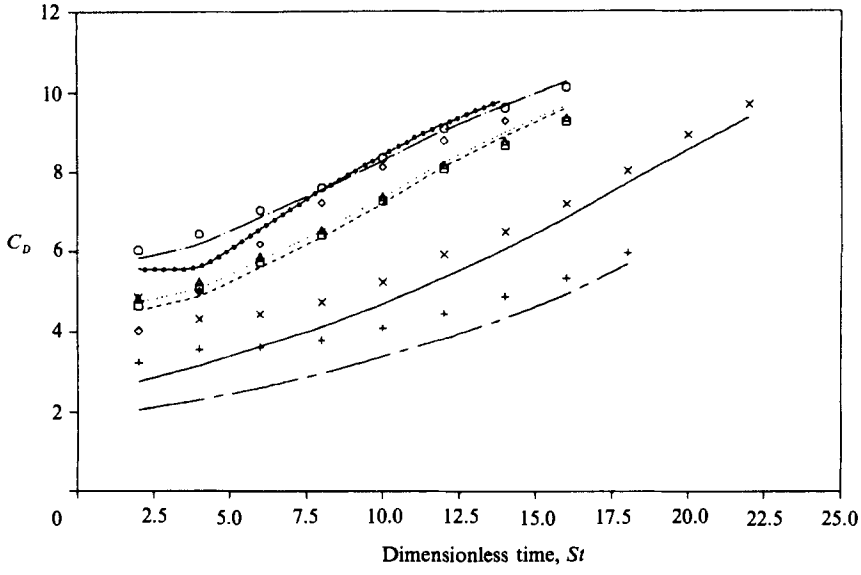

FIGURE 8. Time development of the model coefficient C_D and comparison to fitting function predictions. □, C128R simulation; – – – –, C128R fit prediction; ○, C128S simulation; —·—, C128S fit prediction; △, C128U simulation; · · · · ·, C128U fit prediction; +, C128V simulation; — – —, C128V fit prediction; ×, C128W simulation; ——, C128W fit prediction; ◇, C128X simulation; –•–•–, C128X fit prediction.

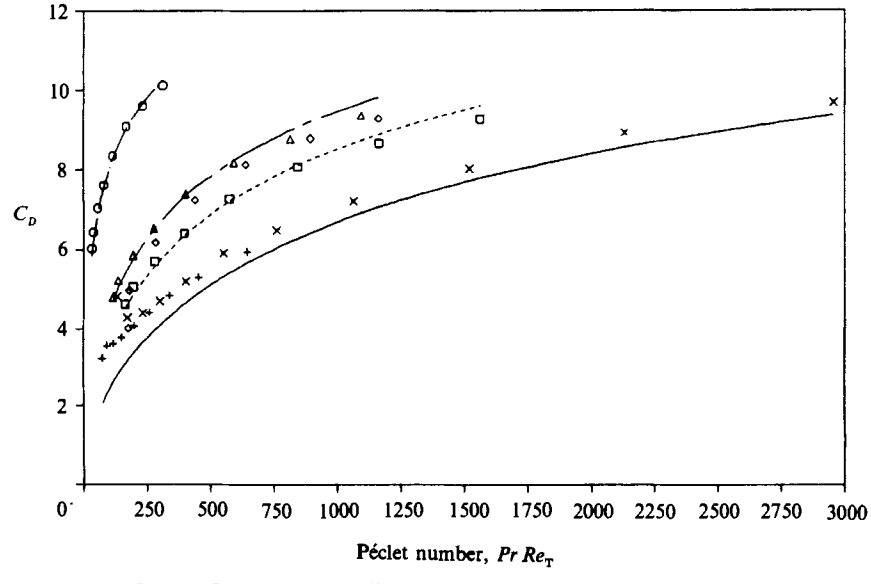

FIGURE 9. Dependence of the model coefficient C_D on the Péclet number with comparison to fitting-function predictions. □, C128R simulation; ○, C128S simulation; △, C128U simulation; +, C128V simulation; ×, C128W simulation; ◇, C128X simulation; – – – –, $Pr = 1.0$ prediction; —·—, $Pr = 0.2$ prediction; — – —, $Pr = 0.7$ prediction; ——, $Pr = 2.0$ prediction.

large Pe is born out by the simulations and might be expected from the non-dimensionalized governing equation for the passive scalar.

The coefficient a_0 is primarily a function of the local turbulent Reynolds number, Re_T. Figure 9 gives evidence of this because data from different simulations at the same Prandtl number lie nearly on a single curve when plotted against Pe (or Re_T since Pr is the same). Because the simulations lead one to believe that many turbulence statistics tend towards a high-Reynolds-number asymptote, a fitting function similar to (3.18) was used for the Reynolds-number dependence,

$$C_D = a_1\left(1+\frac{a_2}{Pe}\right)^{a_3}\left(1+\frac{a_4}{Re_T^{a_5}}\right)^{a_6}. \tag{3.19}$$

The extra degree of freedom a_5 is required to match the correct asymptotic behaviour for both low and high values of Re_T.

The fitting function

$$C_D = 18.0\left(1+\frac{130}{Pe}\right)^{0.25}\left(1+\frac{12.5}{Re_T^{0.48}}\right)^{-2.08} \tag{3.20}$$

gives a reasonable fit to the data and is shown in figures 8 and 9. A poor fit for low St may be expected because these data do not represent developed shear fields and are still affected by the artificial initial conditions. The C128V series data show the poorest agreement, perhaps because the large scales were not adequately captured. The discrepancy between the fit and the data is much less than the scatter among the five individual C_D estimates, implying that more accurate flux predictions would require an alternative model formulation and not simply an improved fitting function (except perhaps for the low Re_T, $Pr = 2.0$ cases as discussed below).

Figure 10 illustrates the ratio of the five non-zero flux components predicted by the model to the corresponding simulated values. 75% of the data points lie within $\pm 20\%$ of perfect agreement. The majority of the points with larger disagreement come from the $Pr = 2.0$ simulations, particularly for low Re_T where the fitting function does a poor job (see figure 9). In general the flux $\overline{\theta_2 u_2}$ tends to be overpredicted and the flux $\overline{\theta_1 u_1}$ tends to be underpredicted. The model also does a fair job of predicting the experimentally observed fluxes of Tavoularis & Corrsin (1981, 1985). The value of C_D given by (3.20) is somewhat below the average of the three experimentally available C_D estimates. The experimental values of $\overline{\theta_2 u_1}$ are predicted to within 9% and the fluxes $\overline{\theta_2 u_2}$ and $\overline{\theta_3 u_3}$ are overpredicted by an amount between 20% and 35%.†

In isotropic turbulence with no mean velocity gradients the model reduces to

$$D_{ij}^{M} = \frac{1}{3C_D}\left(\frac{q^4}{\epsilon}\right)\delta_{ij}. \tag{3.21}$$

The experimental data of Sirivat & Warhaft (1983) for isotropic turbulence with a linear mean scalar gradient yield different values of D_{33} for the same velocity field, depending on the initial conditions of the scalar field. Algebraic models based solely on the velocity field statistics cannot reproduce this behaviour and it is necessary to

† The model developed here corresponds to 'model 2' of Rogers *et al.* (1986). The 'model 1' of that work predicted the scalar flux with about the same accuracy in homogeneous shear flow but failed in the wall region of the turbulent channel flow. 'Model 1' was based on the result, found from the homogeneous shear flow simulations, that in the coordinate system aligned with the principal axes of the Reynolds stress tensor, the D_{ij} tensor assumed a special form with $D_{12} = -D_{21}$.

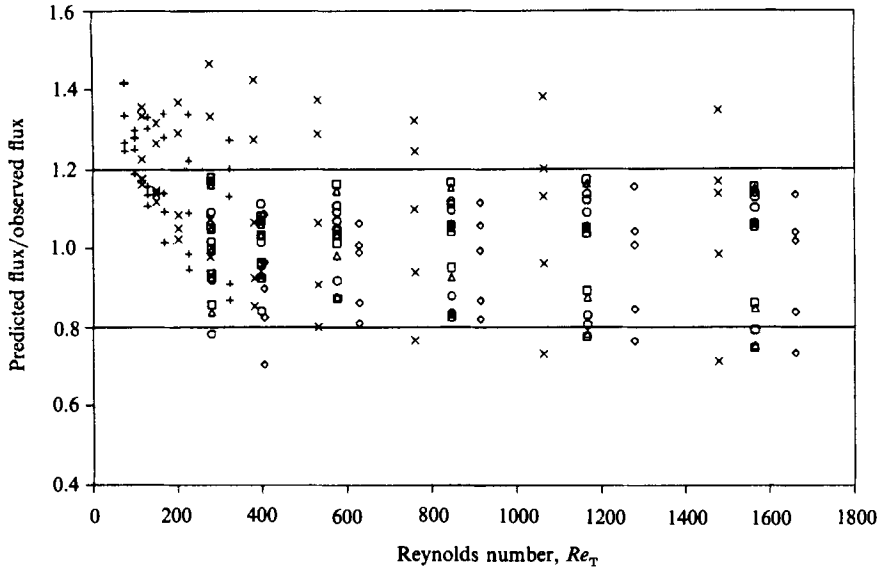

FIGURE 10. Ratio of flux predicted by model to flux calculated from the simulations. Data for all five non-zero flux components. □, C128R simulation; ○, C128S simulation; △, C128U simulation; +, C128V simulation; ×, C128W simulation; ◇, C128X simulation; horizontal lines indicate ±20% discrepancy.

employ ordinary differential equations to predict how the initial conditions affect the scalar flux. Shih & Lumley (1986) have done this and accurately predict the scalar flux in the Sirivat & Warhaft (1983) experiments although this method requires specifying an initial condition (in that work taken at $x/M = 40$ or in one case $x/M = 80$). The model developed here somewhat underpredicts the average of the D_{33} values reported by Sirivat & Warhaft (1983) but does capture the general decrease of D_{33} with x/M as shown in figure 11. Rescaling the curves in figure 11 with the initial-condition information used by Shih & Lumley (1986) would yield agreement comparable with theirs.

4. Model performance in fully developed channel flow

It is often argued that gradient-transport-type models should fail in inhomogeneous flows (e.g. Sreenivasan *et al.* 1981) where the characteristic length of the transporting mechanism is not small compared with the distance over which the mean gradient of the transported property changes appreciably. The universality of the model developed in §3 may therefore be questioned. In order to clarify this issue the model was tested against data from the direct numerical simulations of fully developed turbulent channel flow described in §2.3.

A comparison of the model predictions for the turbulent scalar flux with the corresponding numerically simulated values for the wall transfer (WT) and internal source (IS) cases is shown in figures 12 and 13, respectively. The ability of the model to predict the qualitative nature of the turbulent scalar flux from the wall to the channel centreline for all Prandtl numbers is remarkably good. The fitting function (3.20) could be scaled up slightly to better predict the magnitude of $\overline{\theta u_1}$ but this would typically degrade the accuracy of the $\overline{\theta u_2}$ component. Because $\overline{\theta u_2}$ is the flux

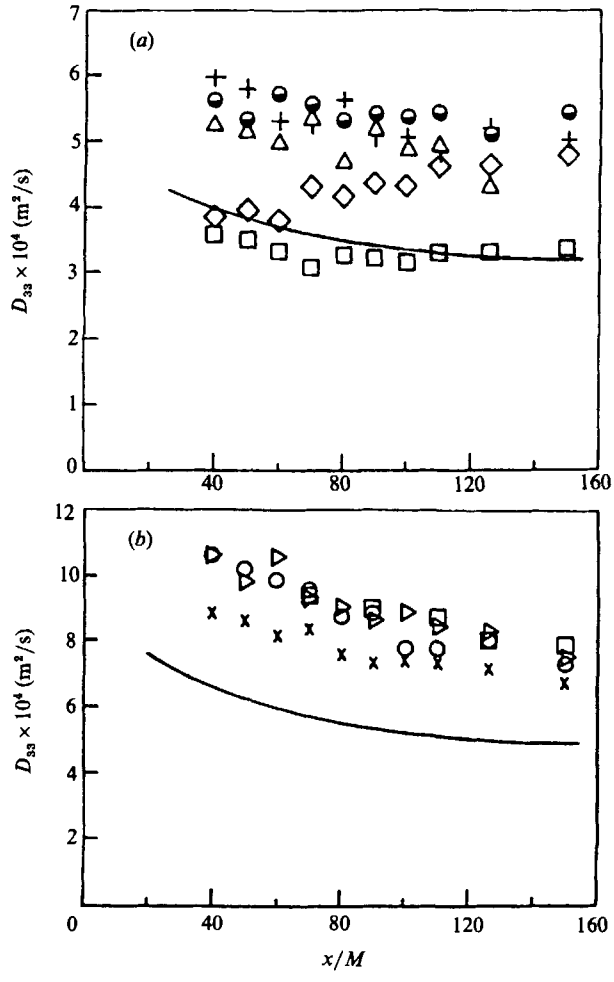

FIGURE 11. Comparison of model predictions with experimental data of Sirivat & Warhaft (1983) in decaying isotropic turbulence. (*a*) $U_\infty = 3.4$ m/s; (*b*) $U_\infty = 6.3$ m/s. Symbols, experimental data; line, model prediction.

component required for closure of the mean scalar equation in the cases considered here, such a modification was not adopted.

The ability of the model to predict the scalar flux from $y/\delta \approx 0.2$ to 0.7 is not entirely unexpected. In this region the channel flow appears to be approximately homogeneous, with little spatial variation of the governing dimensionless parameters (Re_T, Sq^2/ϵ, ω_{rms}/S, ...) and the Reynolds stress anisotropies. This can also be seen from the balance of the terms in the governing equation for the scalar flux. In the region $0.2 \leqslant y/\delta \leqslant 0.7$ the terms due to the inhomogeneity are typically small and the balance qualitatively resembles that of the homogeneous shear flow.

For the passive-scalar fields considered here, (2.8) reduces to

$$0 = -\overline{u_i u_2}\,\overline{T}_{,2} - \overline{\theta u_2}\,\overline{U}_{1,2}\,\delta_{t1} + \psi_i - (0 + \overline{\theta u_i u_2} + \frac{1}{\rho}\overline{p\theta}\delta_{t2} - \nu\overline{\theta u_{i,2}} - \gamma\overline{u_i \theta_{,2}})_{,2}. \quad (4.1)$$

The time derivative of the scalar flux is zero because the channel flow has reached statistical stationarity and therefore the assumption of (3.6) is no longer needed. The

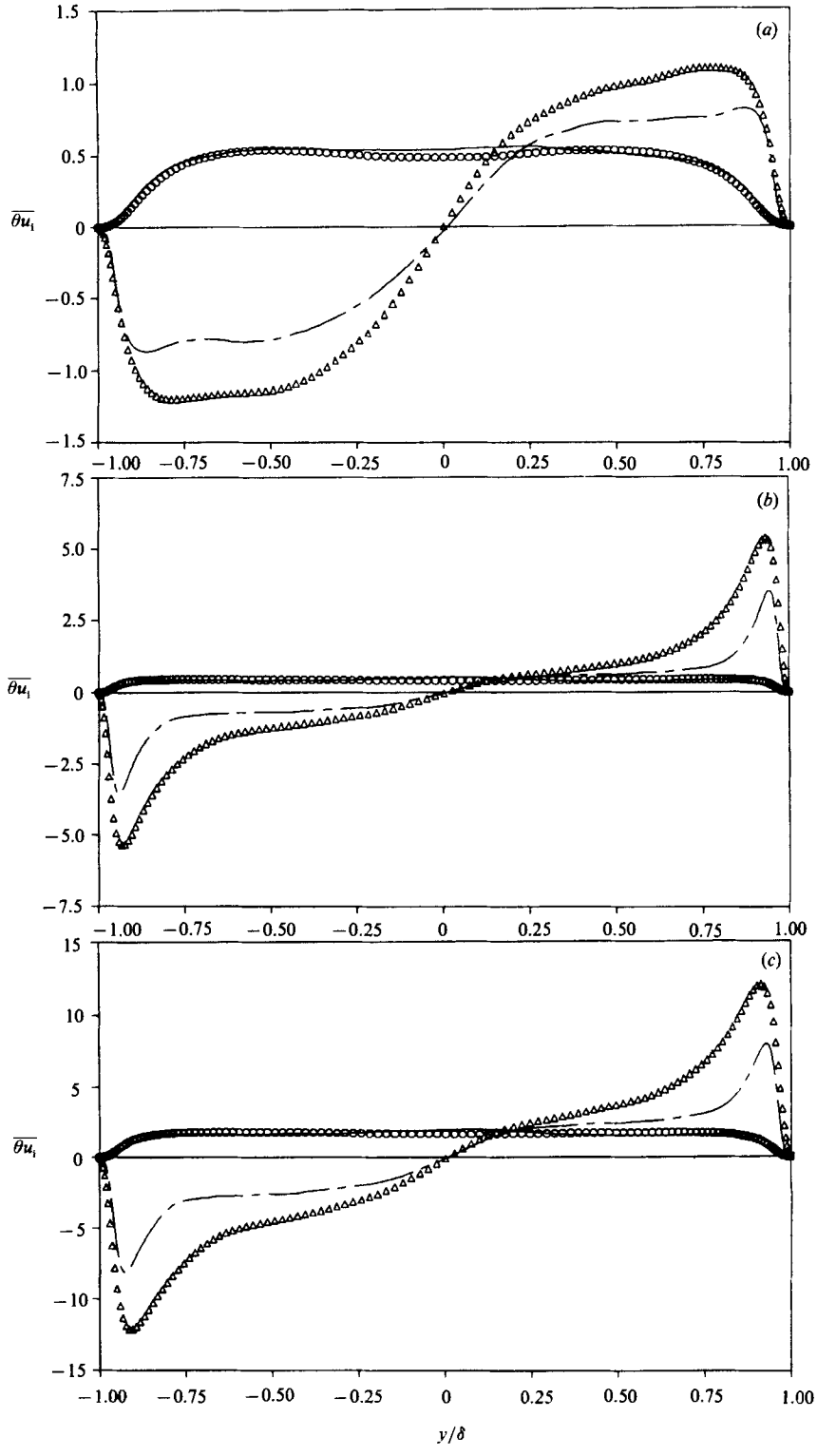

FIGURE 12. Comparison of model scalar flux prediction with numerically simulated scalar flux for WT case of fully developed turbulent channel flow (flux normalized by $u_\tau \theta_\tau = \gamma \overline{T}_{2\text{wall}}$). (*a*) $Pr = 0.1$; (*b*) $Pr = 0.71$; (*c*) $Pr = 2.0$. △, simulated $\overline{\theta u_1}$; — — —, model $\overline{\theta u_1}$; ○, simulated $\overline{\theta u_2}$; ——, model $\overline{\theta u_2}$.

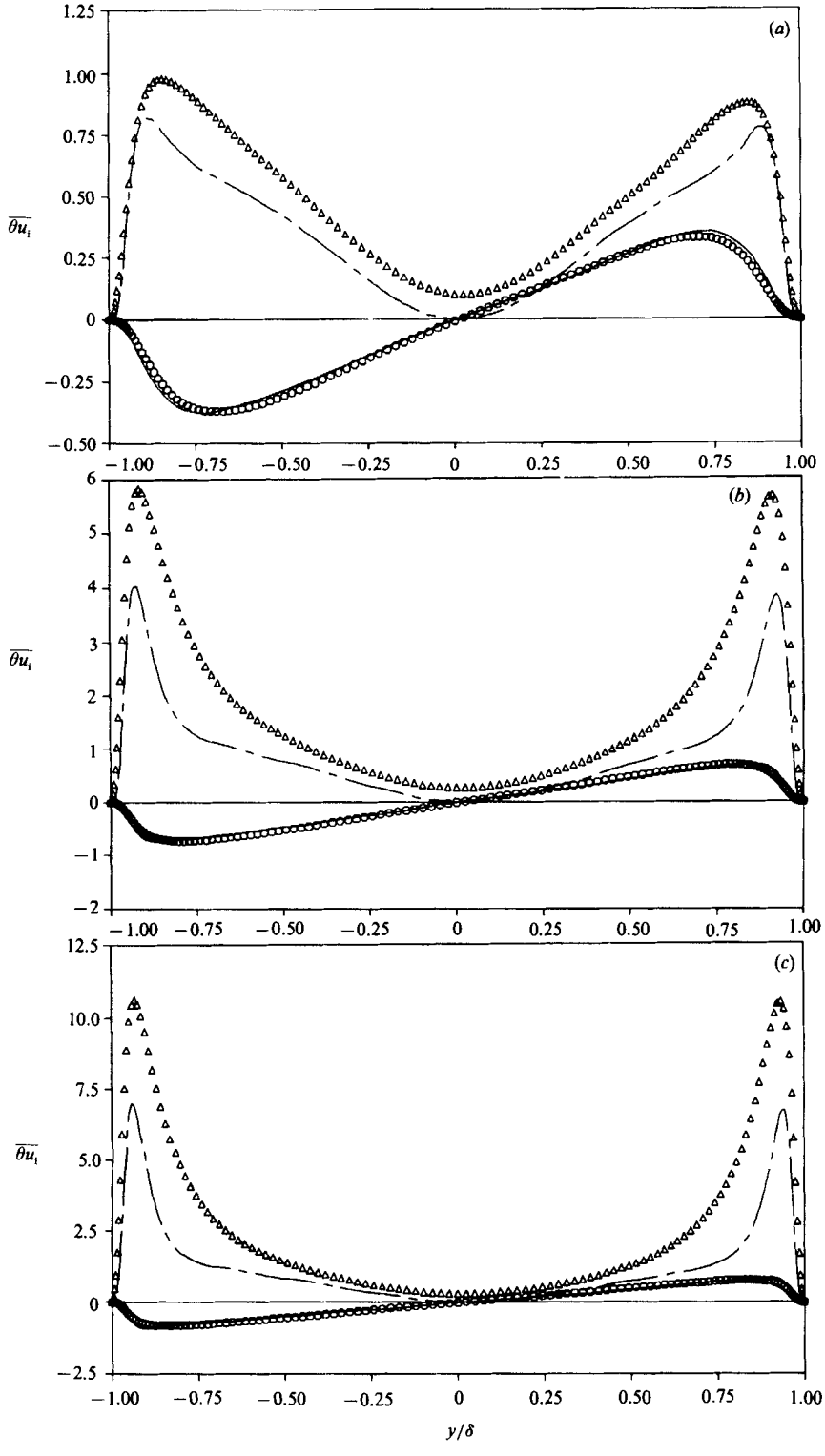

FIGURE 13. Comparison of model scalar flux prediction with numerically simulated scalar flux for IS case of fully developed turbulent channel flow (flux normalized by $u_\tau \theta_\tau = \gamma \overline{T}_{,2\text{wall}}$). (*a*) $Pr = 0.1$; (*b*) $Pr = 0.71$; (*c*) $Pr = 2.0$. △, simulated $\overline{\theta u_1}$; — — —, model $\overline{\theta u_1}$; ○, simulated $\overline{\theta u_2}$; ——, model $\overline{\theta u_2}$.

remaining assumption of the model, that ψ_i is aligned with the scalar flux, holds quite well throughout the entire channel. What is surprising is that the sum of the inhomogeneous terms is also roughly aligned with the scalar flux in regions where this sum is not small (this behaviour is assumed in the algebraic stress model of Gibson & Launder 1976). In fact the sum of all the modelled terms (including those due to inhomogeneities) is typically more aligned with the scalar flux vector than is ψ_i. This alignment maintains itself throughout the channel, including the near-wall region.

The failure of gradient transport models for inhomogeneous flows as discussed by Sreenivasan *et al.* (1981) needs further investigation in the light of the present results. For the inhomogeneous flow they studied, the model developed here predicts

$$-\overline{\theta u_2} = \left(\frac{q^2}{C_D \epsilon}\right) \overline{u_2^2}\, \bar{T}_{,2} - \left(\frac{q^2}{C_D \epsilon}\right) (-\overline{u_1 u_2})\, \bar{T}_{,1}, \tag{4.2}$$

where C_D is given by (3.20). The fact that their experiment did not exhibit a linear relationship between $-\overline{\theta u_2}$ and $\bar{T}_{,2}$ may thus be expected for two reasons. First $\bar{T}_{,1}$ may not be negligible compared with $\bar{T}_{,2}$, particularly near the peak of the temperature profile where $\bar{T}_{,2}$ is zero. Unfortunately, streamwise derivatives are not available from the experiment to check this. Second, variation of C_D in inhomogeneous flows prevents a linear relationship between the scalar flux and the mean gradient even when $\bar{T}_{,1} = 0$.

Sreenivasan *et al.* (1981) find a positive value of $-\overline{\theta u_2}$ at the peak of the temperature profile where $\bar{T}_{,2} = 0$. In this region the mean shear and $-\overline{u_1 u_2}$ are positive and $\bar{T}_{,1}$ is negative due to the spreading of the temperature wake. Equation (4.2) thus predicts the observed sign for the scalar (temperature) flux. Again, lack of streamwise derivative information prevents quantitative comparison.

The experimental data also show a limited region of 'counter-gradient diffusion', or a region where $\overline{\theta u_2}$ and $\partial \bar{T}/\partial x_2$ have the same sign. The suggested fit for C_D cannot predict negative values of C_D and thus the model can only predict counter-gradient diffusion when $\bar{T}_{,1}$ is not equal to zero. Indeed, the counter-gradient diffusion region of the experiments occurs near the peak of the $\bar{T}(x_2)$ profile where, presumably, $\bar{T}_{,1}$ is largest and $\bar{T}_{,2}$ is about zero.

5. Conclusions

Direct numerical simulations of homogeneous turbulent shear flow with mean passive-scalar gradients along each of the coordinate axes have been generated to develop a model for the passive-scalar flux vector. Examination of the terms in the Reynolds-averaged scalar flux balance has shown that the sum of the pressure–scalar gradient and velocity gradient–scalar gradient terms forms a vector approximately aligned with the scalar flux vector itself. Because the time change of the scalar flux is also directed approximately in the direction of the scalar flux for developed shear fields is it possible to derive an algebraic expression for the turbulent scalar flux. The resulting expression is a gradient transport model with a second-rank turbulent diffusivity tensor relating the scalar flux to the mean scalar gradient. The one dimensionless coefficient in the model is fitted as a function of the turbulence Reynolds number and the Péclet number from the simulation results. Using this fitting function the model predicts the scalar flux to within about 20% of the simulated values.

The model developed here has difficulty predicting the turbulent scalar flux when the flux is strongly affected by the initial conditions. Experimental work in decaying

isotropic turbulence with an imposed mean scalar gradient (Sirivat & Warhaft 1983) indicates that different turbulent diffusivities are observed for the same hydrodynamic field depending on the initial conditions of the passive scalar. The algebraic scalar flux model developed here (based solely on the hydrodynamic field, the mean scalar gradient and the Prandtl number) cannot predict this behaviour and underpredicts the average level of the scalar flux. It appears that the production of turbulence by mean shear tends to weaken the effect of the passive-scalar initial conditions and permit the use of an algebraic flux model. Clearly the model would also fail during transients when the flux direction was changing rapidly in time. In such cases and in cases where the turbulent scalar flux is changing from an initially zero value, the assumption made in (3.6) is clearly not valid.

The model was tested against direct numerical simulation results of fully developed turbulent channel flow. Two passive-scalar fields were studied; one with the scalar transferred in at one wall and out the other and one with a uniform internal scalar source and the scalar transferred out of both walls. The model predictions for both cases are in good qualitative agreement with the numerical results, and the flux component required for closure of the mean scalar equation is predicted accurately. The basic assumption of the model, that all terms requiring modelling in the scalar flux balance sum to a vector aligned with the scalar flux itself, was found to hold in this inhomogeneous flow despite the presence of numerous additional terms in the flux balance.

The simple algebraic gradient transport model given by (3.10) and (3.20) is able to predict the turbulent scalar flux in developed shear flows even with the presence of inhomogeneities. By permitting a spatial dependence of the turbulent diffusivity in inhomogeneous flows and recognizing that the turbulent diffusivity is a non-diagonal second-rank tensor, earlier studies indicating the failure of gradient transport models are inconclusive.

We are indebted to Dr John Kim and Professor Parviz Moin for providing the fully developed channel flow data and for their comments during the course of this work.

REFERENCES

BATCHELOR, G. K. 1949 Diffusion in a field of homogeneous turbulence. *Austral. J. Sci. Res.* **A2**, 437–450.

BOUSSINESQ, J. 1877 Essai sur la théorie des eaux courantes. *Mem. Pres. Div. Savants Acad. Sci. Paris* **23**, 46.

CORRSIN, S. 1974 Limitations of gradient transport models in random walks and in turbulence. *Adv. Geophys.* **18A**, 25–60.

GIBSON, M. M. & LAUNDER, B. E. 1976 On the calculation of horizontal, turbulent, free shear flows under gravitational influence. *Trans. ASME* C *J. Heat Transfer* **98**, 81–87.

KAYS, W. M., & CRAWFORD, M. E. 1980 *Convective Heat and Mass Transfer*, 2nd edn. McGraw-Hill.

KIM, J. & MOIN, P. 1987 Transport of passive scalars in a turbulent channel flow. *Proc. 6th Symp. on Turbulent Shear Flows, Toulouse, France, September 7–9, 1987*, pp. 5-2-1–5-2-6.

KIM, J., MOIN, P. & MOSER, R. D. 1987 Turbulence statistics in fully developed channel flow at low Reynolds number. *J. Fluid Mech.* **177**, 133–166.

LAUNDER, B. E. 1978 Heat and mass transport. In *Turbulence* (ed. P. Bradshaw). Topics in Applied Physics, vol. 12, pp. 231–287. Springer.

LEE, M. J. & REYNOLDS, W. C. 1985 Numerical experiments on the structure of homogeneous turbulence. *Dept. Mech. Engng. Rep.* TF-24. Stanford University, Stanford, California.

LUMLEY, J. L. 1978 Computational modelling of turbulent flows. *Adv. Appl. Mech.* **18**, 123–176.

NEWMAN, G. R., LAUNDER, B. E. & LUMLEY, J. L. 1981 Modelling the behaviour of homogeneous scalar turbulence. *J. Fluid Mech.* **111**, 217–232.

ORSZAG, S. A. & PATTERSON, G. S. 1972 Numerical simulation of three-dimensional homogeneous isotropic turbulence. *Phys. Rev. Lett.* **28**, 76–79.

POPE, S. B. 1983 Consistent modeling of scalars in turbulent flows. *Phys. Fluids* **26**, 404–408.

RICHARDSON, L. F. 1920 The supply of energy from and to atmospheric eddies. *Proc. R. Soc. Lond.* A **97**, 354–373.

ROGALLO, R. S. 1977 An ILLIAC program for the numerical simulation of homogeneous incompressible turbulence. *NASA Tech. Mem.* 73203.

ROGALLO, R. S. 1981 Numerical experiments in homogeneous turbulence. *NASA Tech. Mem.* 81315.

ROGERS, M. M. & MOIN, P. 1987 The structure of the vorticity field in homogeneous turbulent flows. *J. Fluid Mech.* **176**, 33–66.

ROGERS, M. M., MOIN, P. & REYNOLDS, W. C. 1986 The structure and modeling of the hydrodynamic and passive scalar fields in homogeneous turbulent shear flow. *Dept. Mech. Engng Rep.* TF-25. Stanford University, Stanford, California.

SHIH, T.-H. & LUMLEY, J. L. 1986 Influence of timescale ratio on scalar flux relaxation: modelling Sirivat & Warhafts homogeneous passive scalar fluctuations. *J. Fluid Mech.* **162**, 211–222.

SHIRANI, E., FERZIGER, J. H. & REYNOLDS, W. C. 1981 Mixing of a passive scalar in isotropic and sheared homogeneous turbulence. *Dept. Mech. Engng Rep.* TF-15. Stanford University, Stanford, California.

SIRIVAT, A. & WARHAFT, Z. 1983 The effect of a passive cross-stream temperature gradient on the evolution of temperature variance and heat flux in grid turbulence. *J. Fluid Mech.* **128**, 323–346.

SREENIVASAN, K. R., TAVOULARIS, S. & CORRSIN, S. 1981 A test of gradient transport and its generalizations. In *Turbulent Shear Flows 3* (ed. L. J. S. Bradbury, F. Durst, B. E. Launder, F. W. Schmidt & J. H. Whitelaw), pp. 96–112. Springer.

TAVOULARIS, S. & CORRSIN, S. 1981 Experiments in nearly homogeneous turbulent shear flow with a uniform mean temperature gradient. Part 1. *J. Fluid Mech.* **104**, 311–347.

TAVOULARIS, S. & CORRSIN, S. 1985 Effects of shear on the turbulent diffusivity tensor. *Intl J. Heat Mass Transfer* **28**, 265–276.

ZEMAN, O. & LUMLEY, J. L. 1979 Buoyancy effects in entraining turbulent boundary layers: a second-order closure study. In *Turbulent Shear Flows 1* (ed. F. Durst, B. E. Launder, F. W. Schmidt & J. H. Whitelaw), pp. 295–305. Springer.